Supporting Information for

"Towards building a physical proxy for gas-phase sulfuric acid concentration based on its budget analysis in polluted Yangtze River Delta, east China"

Liwen Yang[1,2], Wei Nie[1,2,*], Yuliang Liu[1,2], Zhengning Xu[1,2], Mao Xiao[3], Ximeng Qi[1,2], Yuanyuan Li[1,2], Ruoxian Wang[1,2], Jun Zou[1,2], Pauli Paasonen[4], Chao Yan[4], Zheng Xu[1,2], Jiaping Wang[1,2], Chen Zhou[1,2], Jian Yuan[1,2], Jianning Sun[1,2], Xuguang Chi[1,2], Veli-Matti Kerminen[1,4], Markku Kulmala[1,4], Aijun Ding[1,2]

[1]Joint International Research Laboratory of Atmospheric and Earth System Sciences, School of Atmospheric Sciences, Nanjing University, Nanjing, China

[2] Jiangsu Provincial Collaborative Innovation Center of Climate Change, Nanjing, 210023, China

[3] Laboratory of Atmospheric Chemistry, Paul Scherrer Institute, 5232 Villigen, Switzerland

[4] Institute for Atmospheric and Earth System Research / Physics, Faculty of Science, University of Helsinki, Finland

*Corresponding to: Wei Nie (niewei@nju.edu.cn)

Supplementary Text, Figure captions and Table

Text S1 Measurements of sulfuric acid

H_2SO_4 was measured by an Aerodyne chemical ionization mass specrometer (CIMS) equipped with a nitrate chemical source. This technique has been previously descibed elsewhere [1].In this study,sampling took place througth a stainless-steel tube with a length of 1 m and 1.5 m above the ground level. Note that measurements of H_2SO_4 during spring were conducted outside the building at the 5th floor, with a distance of about 200 m to SORPES, and the H_2SO_4 concentration can be regarded as consistent with it in SORPES.

The signals of H_2SO_4 monomer and dimer are identified by defining the exact mass of HSO_4^-, $H_2SO_4NO_3^-$ and $H_2SO_4HSO_4^-$.And the quantification of them is seasonal calibrated with the known concentration of H_2SO_4 calculated from the SO_2-OH reaction [2]. The calibration coefficients obtained were 5.22×10^9 cm^{-3}in winter, 7.27×10^9 cm^{-3}in spring, 3.92×10^9 cm^{-3} in summer, and 4.6×10^9 cm^{-3} in autumn,with diffusion losses in tube into consideration.

Text S2 Estimation of the hydroxyl radical

In the nonlinear proxy based on statistical analysis method,we replaced OH with the UVB radiation intensity as in previous works. UVB was measured by a radiometer (Kipp&Zonen UVS-B-T). And in the physical proxy, we computed the photolysis frequency J(O^1D) using the Tropospheric Ultraviolet and Visible (TUV) radiation model (https://www2.acom.ucar.edu/modeling/tropospheric-ultraviolet-and-visible-tuv-radiation-model) and corrected the simulated results by observed UVB [3]. The daytime OH concentration was calculated by applying the empirical formula proposed by Rohrer and Berresheim[4], which can be described by the follwing equation:

$$[OH] = a \times (^{J(O^1D)}/_{10^{-5}s^{-1}})^b + c$$

Here,the pre-exponential coefficient, a, reflects the dependence of OH on reactants such as NOx, VOCs, O_3 or H_2O.The exponent b reflects the combined effects of all photolytic processes and it was observed to be around 1 in various environments. The coefficient c reflects the OH production from all light-independent processes, which has already been included in the alkene ozonolysis term. In order to simplify the discussion,we assume that b is 1 in this study. Table S5 summarizes the coefficients a and b in OH observations when b varies from 0.9 to 1.1.

Text S3 Calculation of condensation sink

The condensation sink is regarded as H_2SO_4 loss on pre-existing aerosol. It can be calculated by the following equation [5]:

$$CS = 4\pi D \int_0^{d_p max} \beta_m(d_p')d_p' N_{d_p'} dd_p' = 4\pi D \sum_{d_p'} \beta_{m,d_p'} d_p' N_{d_p'}$$

The particle number size distribution between 6-800 nm was measured using a Differential Mobility Particle Sizer (DMPS) [6]. We further tested the contributions of sub-6nm particles and particles larger than 800 nm to CS based on measurements with a Scanning Mobility Particle Sizer (SMPS, 4-495.8 nm) and Aerodynamic Particle Sizer (APS, 0.54-19.8 μ m) from January 1, 2019 to June 30, 2019.The correlation between the CS calculated from the size ranges 4-19800 nm and 6-800 nm was almost linear and close to the 1:1 line (Figure S4). Half of the $CS_{4\text{-}19800nm}/CS_{6\text{-}800nm}$ ratios were lower than 1.028 and 85% of the ratios were lower than 1.095,

indicating that the contribution from particles outside the range of 6-800 nm is generally negligible. It should be noted that we take hygroscopic growth correction into consideration when calculating the CS, as has been previously described in Wu et al.[7].

Text S4 Calculation of dry deposition

Dry deposition, as the ultimate path by which trace gases and particles are removed from the atmosphere in the absence of precipitation, is governed by three factors: atmopheric turbulence, the physical and chemical properties of the depositing species, and the nature of the surface. Since simulating such a variety of complex processes is gernerally impratical, dry deposition is usually simplified as a single parameter, the deposition velocity(v_d). For gases,V_d in existing dry deposition models is computed from a formula analogous to Ohm's law in electrical circuits [8]:

$$V_d^i=(R_a+R_b^i+R_c^i)^{-1}$$

The term R_a represents aerodynamic resistance and is governed by turbulent transport. This term has the same value for all species, and it can be calculated using the following equation [9]:

$$R_a=\begin{cases}\frac{1}{ku_*}\left[\ln\left(\frac{z}{z_0}\right)+4.7(\xi-\xi_0)\right](for \quad 0<\xi<1)\\ \frac{1}{ku_*}\left[\ln\left(\frac{z}{z_0}\right)\right](for \quad \xi=0)\\ \frac{1}{ku_*}\left[\ln\left(\frac{z}{z_0}\right)+\ln\left(\frac{(\eta_0^2+1)(\eta_0+1)^2}{(\eta_r^2+1)(\eta_r+1)^2}\right)+2(tan^{-1}\eta_r-tan^{-1}\eta_0)\right](for \quad -1<\xi<0)\end{cases}$$

Here, z is 1.5 m where H_2SO_4 measurements were conducted and the height where we calculate V_d, k is the von Karman constant usually set to 0.4, z_0 is the roughness length, and ξ is dimensionless height scale (z/L),where L is the Monin-Obukhov length. Next, η_r and η_0 can be calculated using the following equation :

$$\eta_0=(1-15\xi_0)^{1/4},\ \eta_r=(1-15\xi_r)^{1/4}$$

In order to simplify the discussion,we assumed L=100 m and z_0=0.17 m. u* is the friction velocity, which can be obtained from real-time measurements by the eddy-convariance system (EC3000,Campbell Scientific), including a three-dimensional sonic anemometer (CSAT3) and an infrared analyzer (LI7500) at the height of 3 m. For more details, see for example [10]

The term R_b^i represents the quasi-laminar resistance dependent on molecular properties of the substance and surface characteristics. A useful expression for r_b for gases is

$$R_b=\frac{5Sc^{2/3}}{u_*}$$

Here, Sc is the dimensionless Schmidt number (Sc=ν/D), where ν is the kinematic viscosity of air and D is the molecular diffusivity of the species. For H_2SO_4, D decreases with an increasing relative humudity and has a rather strong temperature dependence [11]. In this study, Sc was set to 3.5, which was the intermediate value in our observation environment.

The surface resistance R_c consists of three parts: the vegetation resistance, the lower canopy resistance, including transfering by buoyant convenction and uptaking by leave, twings, etc., and the ground resistance which depends on the properties of a surface [12]. Therefore, this term shows a large variation with types of surface and depisition species. However, since Henry's law coefficient of H_2SO_4 is extemely high, up to 1.3×10^{15}M atm^{-1} [13], this term becomes

negligible compared with the other two terms.

Figures

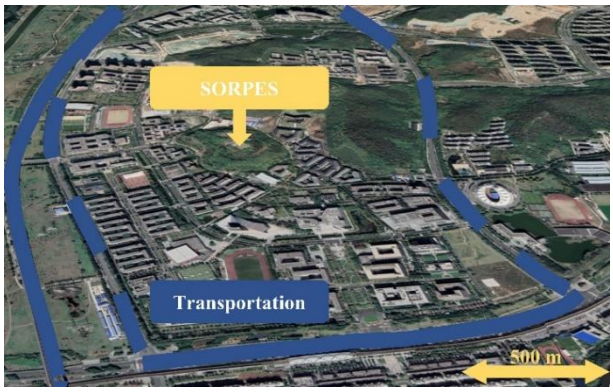

Figure S1. The map of the measurement site. The yellow arrow points to the site location. Two solid blue lines indicate busy roads, and two dashed blue lines indicate less busy roads

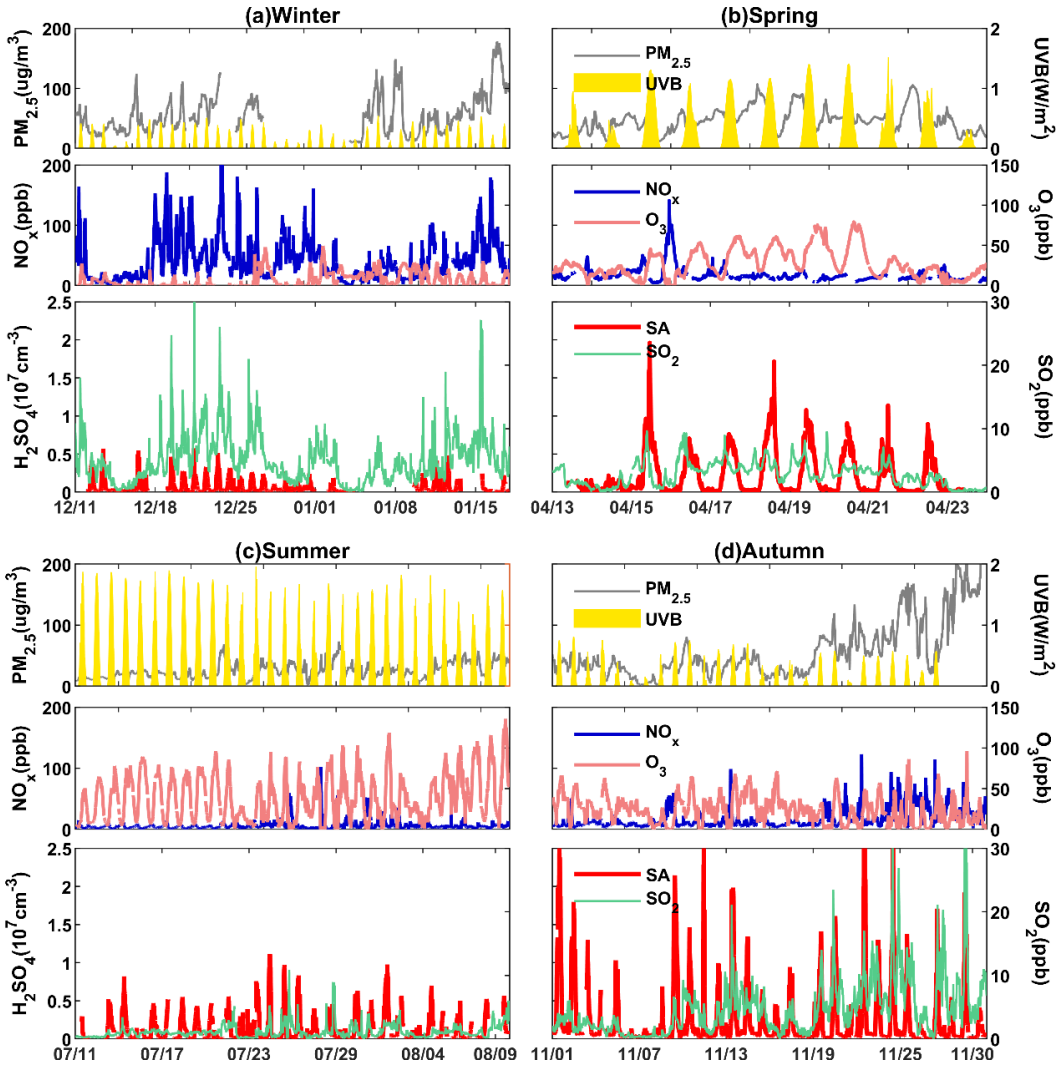

Figure S2. Time series of gaseous H_2SO_4 and related parameters in (a)winter, (b)spring, (c)summer and (d)autumn, respectively.

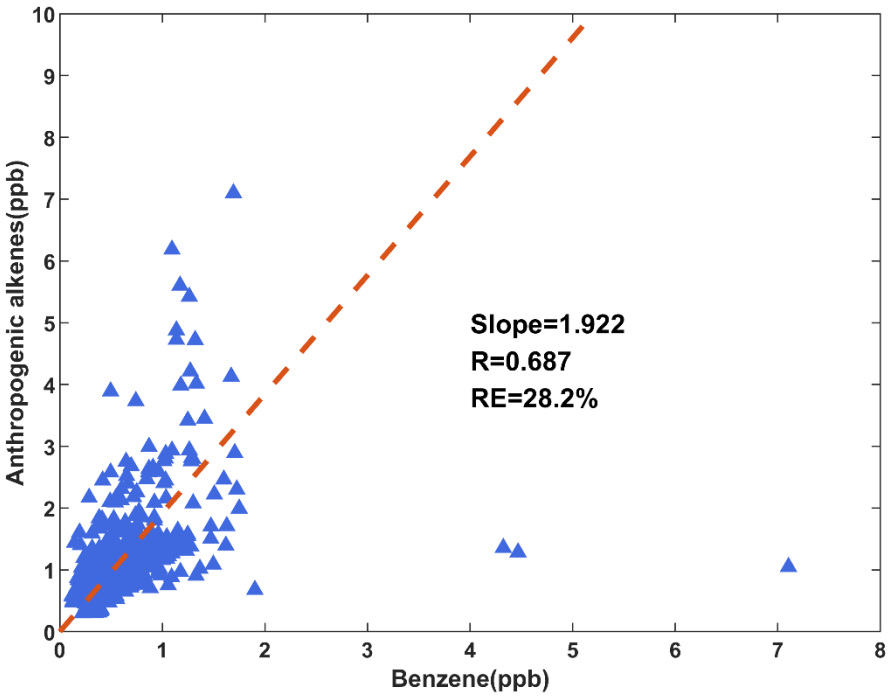

Figure S3. Relationship between dominating anthropogenic alkenes and benzene during 26th November 2019 to 4th January 2020.Correlation coefficient R (Spearman type) is 0.687 and relative error is 28.2%. The orange line represents a linear fit with a zero intercept and its slope is 1.922.

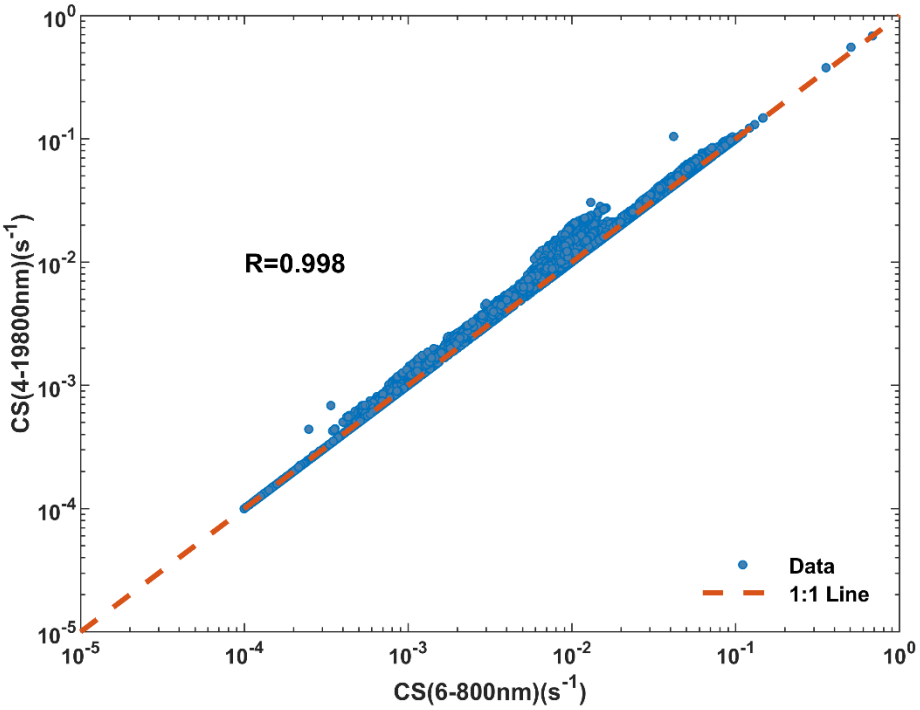

Figure S4. Correlation between CS contributed from 6-800 nm and 4-19800nm particles during January 1, 2019 to June 30, 2019.Correlation coefficient R is in Pearson type.

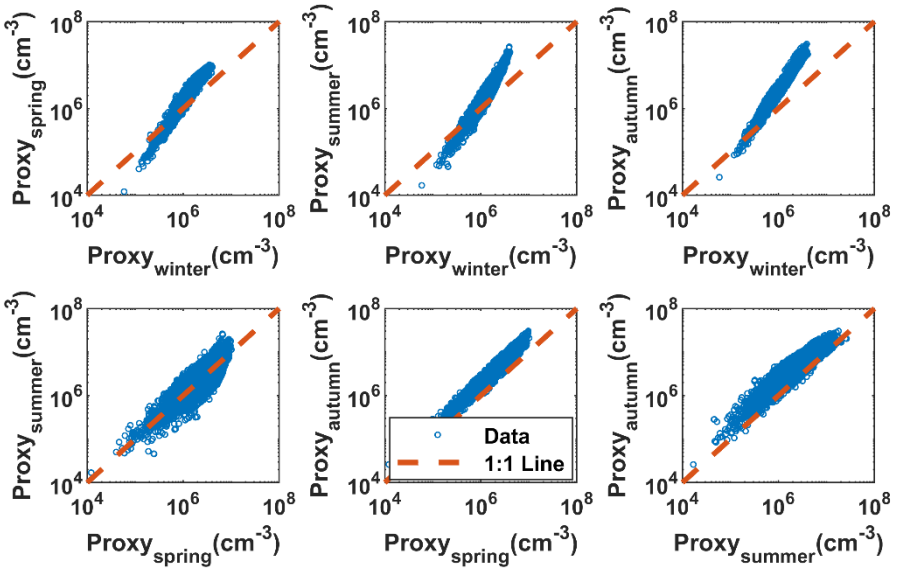

Figure S5. Relationship between H_2SO_4 estimated by different proxies based on the empirical formulas in different season. The coefficients of each proxy are listed in Table S1.

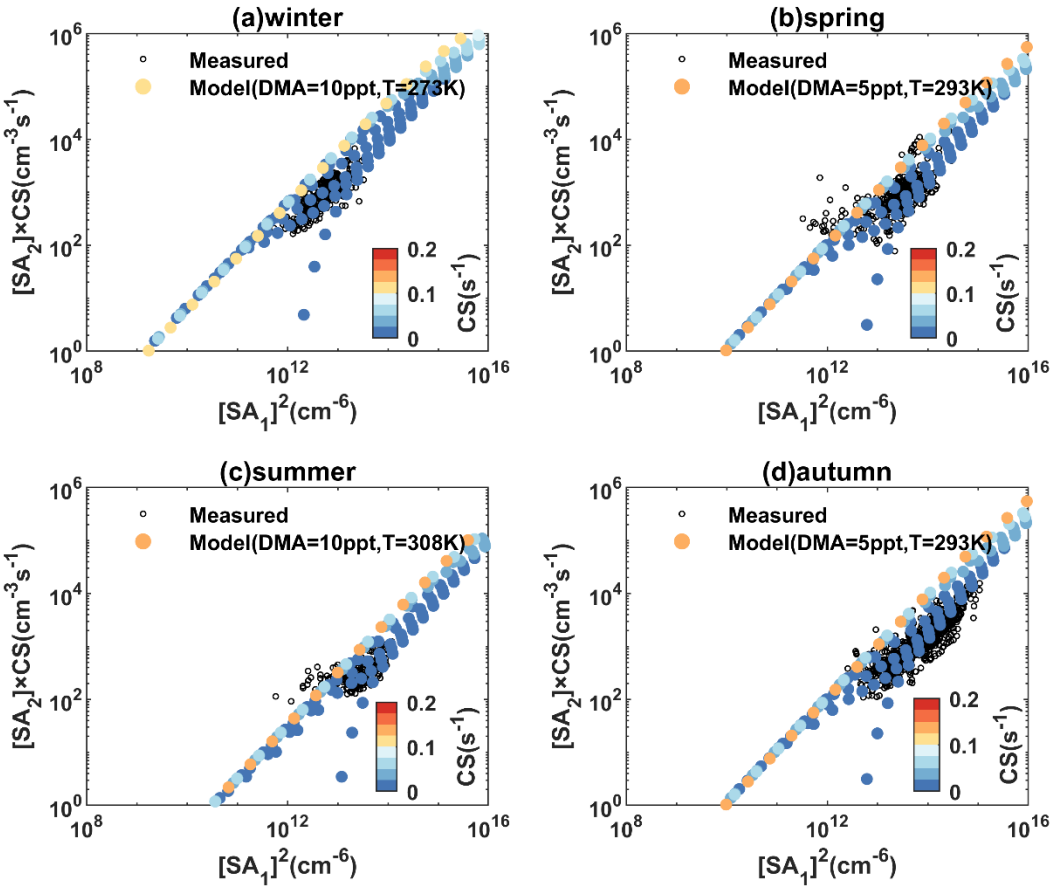

Figure S6. Comparison between daytime data in four seasons and simulations under different temperatures and DMA concentration. Measurements in summer and autumn are similar to the simulations with 10 ppt DMA, while spring and autumn with 5 ppt DMA

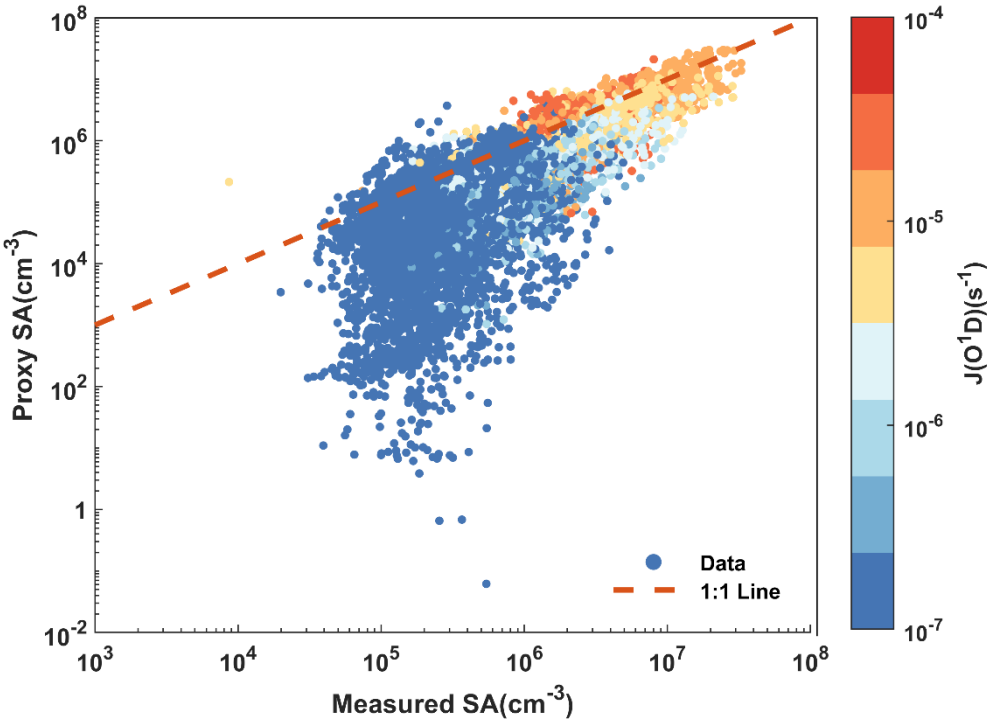

Figure S7. Relationship between proxy SA without emissions into consideration and measured SA. Points are colored with J(O^1D) to differentiate H_2SO_4 in daytime and nighttime. Different coefficients are used in different seasons, which are listed in Table S3.

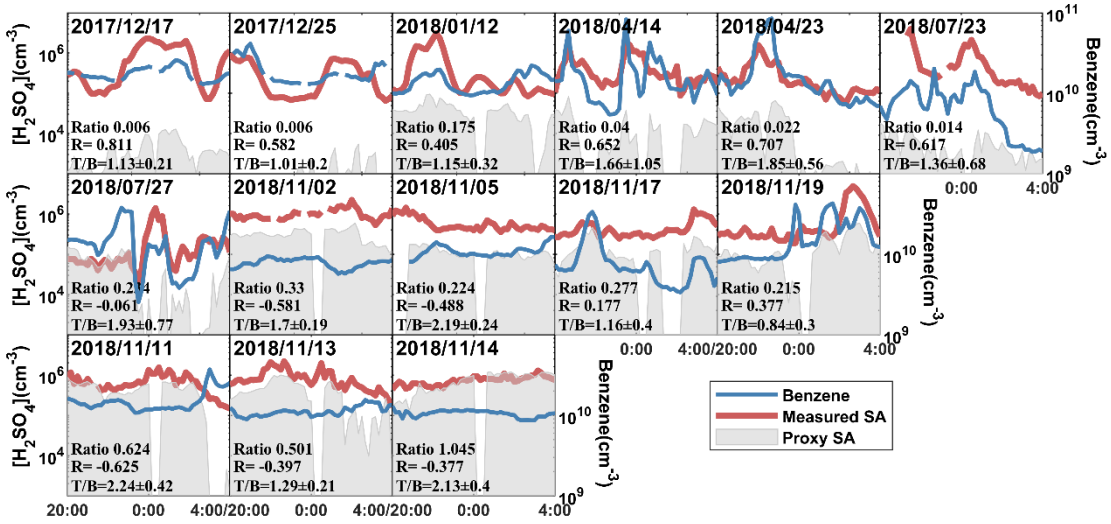

Figure S8. Time series measured SA, simulated SA and Benzene during selected nighttime H_2SO_4 events. The top panel shows events when H_2SO_4 and benzene have similar variation. The bottom panel shows events, which can be explained by alkenes ozonolysis source. The middle panel shows undistinguished events, which could be contributed by both direct emission, alkenes ozonolysis and other unknown sources. Here, ratio represents the level which can be explained by sCI-SO_2 reactions, R is the correlation coefficient between benzene and gaseous H_2SO_4, and T/B denotes the toluene to benzene ratio with 1σ errors. Events which can be explained by the source of alkene ozonolysis source are defined by ratio>0.5, while emission source by ratio<0.25 and R>0.4. Proxy SA was simulated by Eq8. K_1 in four seasons are listed in Table S3.

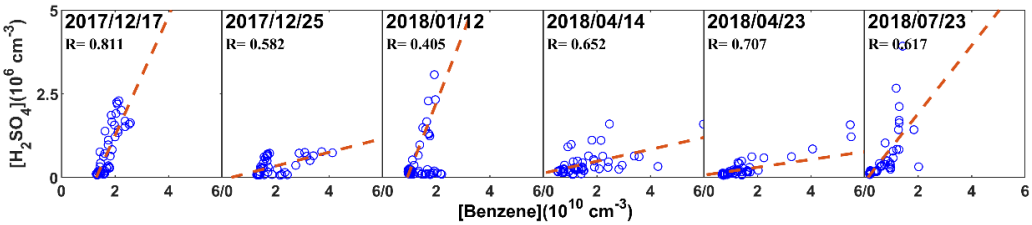

Figure S9. Relationship between H_2SO_4 and benzene in emission cases. R is the correlation coefficient in Spearman type). The orange line in each subgraph represents a linear fit.

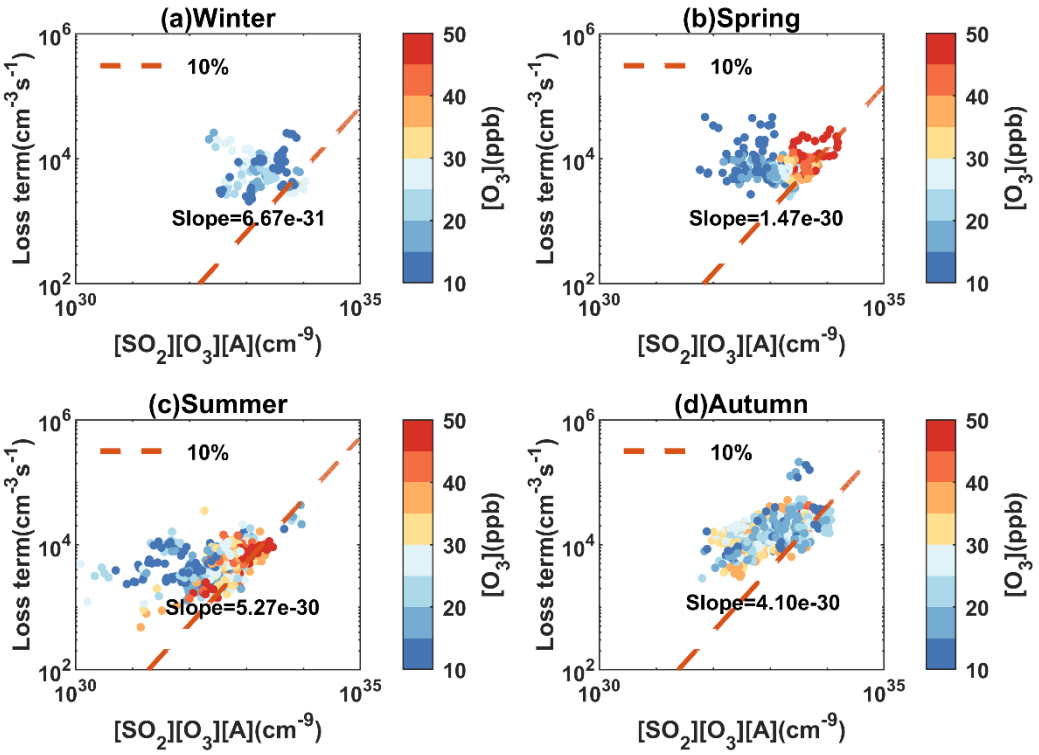

Figure S10. Relationship between loss term of nighttime H_2SO_4 and the source term([SO_2] *[O_3] *[Alkenes]) based on points with O_3 concentration higher than 10ppb for(a)winter, (b)spring, (c)summer, and (d)autumn. The orange dotted line in each subgraph represents the 10^{th} percentiles of slopes of seasonal points.

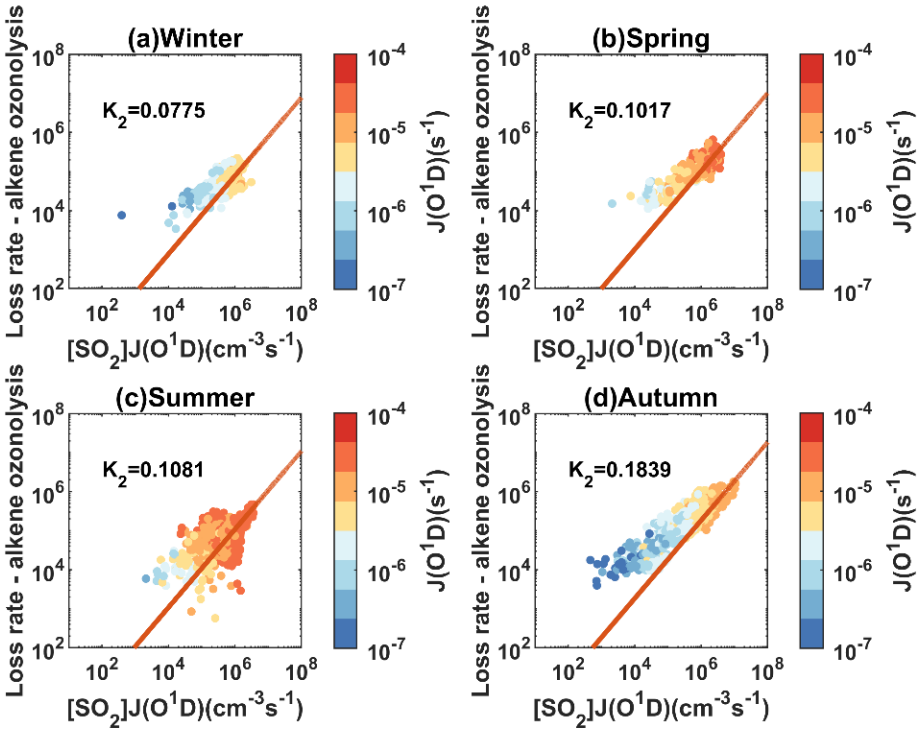

Figure S11. Daytime relationship between light-dependent source term([SO_2] *J(O^1D)) and sink term which subtracts production rate contributed via SO_2-sCI reaction. The orange line in each subgraph represents a linear fit with a zero intercept.

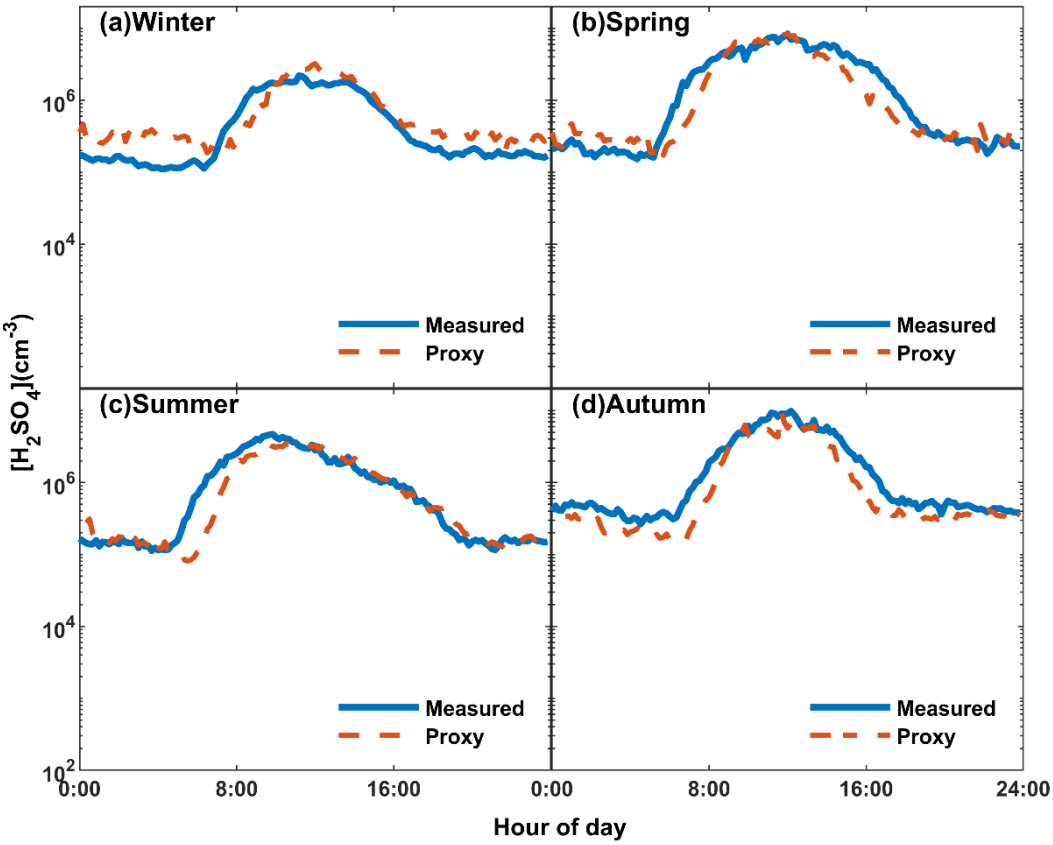

Figure S12. Diurnal variations of measured H_2SO_4 and H_2SO_4 obtained from respective steady-state equilibrium method with emissions into consideration in (a)winter, (b)spring, (c)summer, and (d)autumn (Eq8). Coefficients in four seasons are listed in Table S4.

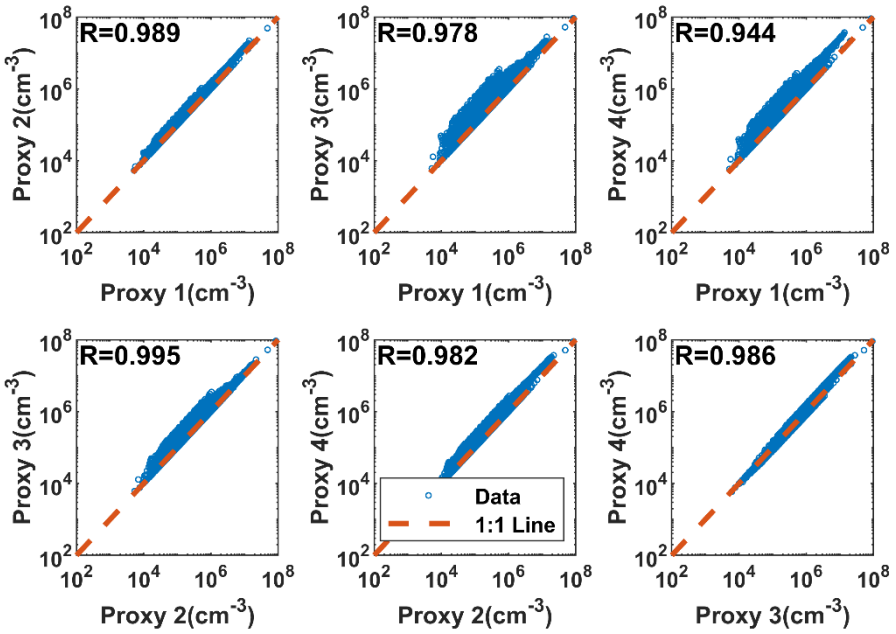

Figure S13. Correlation between H_2SO_4 estimated by physical proxies in different season (Eq8). The coefficients of each proxy are listed in Table S4. Correlation coefficients(R) are in Pearson type.

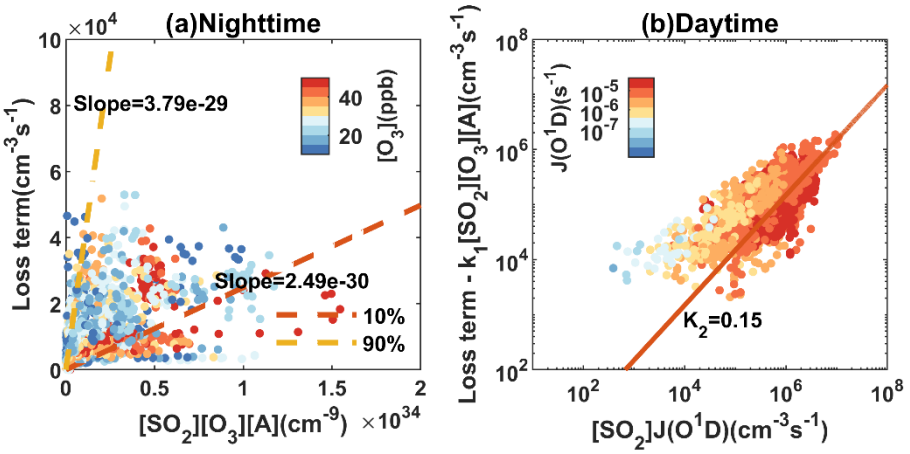

Figure S14. (a)Relationship between loss term of nighttime H_2SO_4 and the source term([SO_2] *[O_3] *[Alkenes]) based on points with O_3 concentration higher than 10ppb during total period. The orange and yellow dotted lines in the subgraph represent the 10th and 90th percentiles of slopes of points. (b) Daytime relationship between light-dependent source term([SO_2] *J(O^1D)) and sink term which subtracts production rate contributed via SO_2-sCI reaction. The orange line in the subgraph represents a linear fit with a zero intercept.

Tables

Table S1. Results of the nonlinear fitting procedure for proxy function: $SA=k_0[SO_2]^a CS^b UVB^c$ in daytime and comparison with previous works. $[SO_2]$ is Sulphur dioxide concentration in cm^{-3}, CS is the condensation sink in s^{-1} and UVB is the intensity of ultraviolet radiation b in $W\ m^{-2}$

Location	K_0	a	b	c	Ref
NJ($Proxy_{winter}$)	579.30	0.31	-0.14	0.35	This work
NJ($Proxy_{spring}$)	2.33×10^3	0.30	-0.10	0.64	
NJ($Proxy_{summer}$)	0.01	0.73	-0.46	0.48	
NJ($Proxy_{autumn}$)	26.04	0.45	-0.50	0.60	
SPC	$K*9.0\times10^{-4}$	0.69	-0.26	0.90*	1
Melpitz	$K*4.7\times10^{-4}$	0.74	-0.18	0.87*	
Hyytiälä[A]	$K*1.2\times10^{-2}$	0.61	-0.03	0.84*	
Hyytiälä[B]	$K*2.23\times10^{-6}$	0.81	-0.46	1.05*	
NWR	$K*2.45\times10^{-2}$	0.88	0.41	0.17*	
Atlanta	$K*4.52\times10^{-2}$	0.48	0.18	1.41*	
HPB	$K*9.48\times10^{-5}$	0.73	-0.58	0.77*	
BJ	515.74	0.38	0.03	0.14	2

1:[14].

SPC: San Pietro Capofiume, Italy (Rural), 21.6-16.7.2009;

Melpitz, Germany (Rural), 30.4-31.5.2008;

Hyytiälä, Finland (Forest), A:17.3-13.4.2003; B:24.3-28.6.2007);

NWR: Niwot Ridge, Colorado USA(Forest): 24.6-15.7.2007;

Atlanta, Georgia USA(Urban):30.7-31.8.2002;

HPB: Hohenpeissenberg, Germany (Mountain): 1.4.1998-31.7.2000.

2:[15].BJ: Beijing, China(Urban):9.2.2018-14.3.2018

K is temperature-dependent reaction constant descried in [14]

*: OH concentration was represented by global radiation instead of UVB.

Table S2. Relative error of traditional proxies.

	$Proxy_{winter}$	$Proxy_{spring}$	$Proxy_{summer}$	$Proxy_{autumn}$
Winter	36%	65%	156%	240%
Spring	52%	30%	33%	103%
Summer	44%	53%	35%	138%
Autumn	67%	53%	33%	37%

Table S3. Coefficients of steady-state equilibrium method. Proxy1,2,3,4 represent results for winter, spring, summer and autumn, respectively. K_1 are based on nighttime H_2SO_4 of each season and K_2 are obtained by correlation between $[SO_2]$ *$J(O^1D)$ term and sink term, which subtracts production rate contributed by SO_2-sCI reaction. In proxy, gases are in cm^{-3} and $J(O^1D)$ is in s^{-1}.

	Proxy1	**Proxy2**	**Proxy3**	**Proxy4**
$K_1(cm^6s^{-1})$	2.50e-30	2.21e-30	5.91e-30	5.86e-30
K_2	5.82e-2	10.09e-2	10.52e-2	18.00e-2
β (cm^3s^{-1})	5.69e-10	1.37e-10	2.55e-11	1.15e-10

Table S4. Coefficients based on seasonal data with O_3 concentration higher than 10ppb. Proxy1,2,3,4 represent results for winter, spring, summer and autumn, respectively. In proxy, gases are in cm^{-3} and $J(O^1D)$ is in s^{-1}.

	Proxy1	**Proxy2**	**Proxy3**	**Proxy4**
$K_1(cm^6s^{-1})$	6.67e-31	1.47e-30	5.27e-30	4.10e-30
K_2	7.75e-2	10.17e-2	10.81e-2	18.38e-2
β (cm^3s^{-1})	5.69e-10	1.37e-10	2.55e-11	1.15e-10

Table S5. Summary of the coefficients a and b in observations.

Location	Type	a	b	Ref
Pabstthum, Germany	Rural/Urban	2	0.92	[16]
Hohenpeissenberg, Germany	Rural	2.4	0.93	[4]
54°N,12°E Germany	Rural	3.9	0.95	[17]
Guangzhou, China	Rural	4	1	[18]
Beijing, China	Suburban	4	1	[19]
Beijing, China	Suburban	4.33	1	[20]
Wangdu, China	Rural	4.5	1	[21]
Beijing, China	Urban	4.81	1	[22]

Supplementary references

1. Jokinen, T.; Sipila, M.; Junninen, H.; Ehn, M.; Lonn, G.; Hakala, J.; Petaja, T.; Mauldin, R. L.; Kulmala, M.; Worsnop, D. R., Atmospheric sulphuric acid and neutral cluster measurements using CI-APi-TOF. *Atmospheric Chemistry and Physics* **2012,** *12*, (9), 4117-4125.
2. Kurten, A.; Rondo, L.; Ehrhart, S.; Curtius, J., Calibration of a Chemical Ionization Mass Spectrometer for the Measurement of Gaseous Sulfuric Acid. *J. Phys. Chem. A* **2012,** *116*, (24), 6375-6386.
3. Liu, Y. L.; Nie, W.; Xu, Z.; Wang, T. Y.; Wang, R. X.; Li, Y. Y.; Wang, L.; Chi, X. G.; Ding, A. J., Semi-quantitative understanding of source contribution to nitrous acid (HONO) based on 1 year of continuous observation at the SORPES station in eastern China. *Atmospheric Chemistry and Physics* **2019,** *19*, (20), 13289-13308.
4. Rohrer, F.; Berresheim, H., Strong correlation between levels of tropospheric hydroxyl radicals and solar ultraviolet radiation. *Nature* **2006,** *442*, (7099), 184-187.
5. Kulmala, M.; Petaja, T.; Nieminen, T.; Sipila, M.; Manninen, H. E.; Lehtipalo, K.; Dal Maso, M.; Aalto, P. P.; Junninen, H.; Paasonen, P.; Riipinen, I.; Lehtinen, K. E. J.; Laaksonen, A.; Kerminen, V. M., Measurement of the nucleation of atmospheric aerosol particles. *Nat. Protoc.* **2012,** *7*, (9), 1651-1667.
6. Wiedensohler, A.; Birmili, W.; Nowak, A.; Sonntag, A.; Weinhold, K.; Merkel, M.; Wehner, B.; Tuch, T.; Pfeifer, S.; Fiebig, M.; Fjaraa, A. M.; Asmi, E.; Sellegri, K.; Depuy, R.; Venzac, H.; Villani, P.; Laj, P.; Aalto, P.; Ogren, J. A.; Swietlicki, E.; Williams, P.; Roldin, P.; Quincey, P.; Huglin, C.; Fierz-Schmidhauser, R.; Gysel, M.; Weingartner, E.; Riccobono, F.; Santos, S.; Gruning, C.; Faloon, K.; Beddows, D.; Harrison, R. M.; Monahan, C.; Jennings, S. G.; O'Dowd, C. D.; Marinoni, A.; Horn, H. G.; Keck, L.; Jiang, J.; Scheckman, J.; McMurry, P. H.; Deng, Z.; Zhao, C. S.; Moerman, M.; Henzing, B.; de Leeuw, G.; Loschau, G.; Bastian, S., Mobility particle size spectrometers: harmonization of technical standards and data structure to facilitate high quality long-term observations of atmospheric particle number size distributions. *Atmos. Meas. Tech.* **2012,** *5*, (3), 657-685.
7. Wu, Y.; Yin, Y.; Gu, X.; Tan, H., An observational study of the hygroscopic properties of aerosols in north suburb of Nanjing. *China Environmental Science* **2014,** *34*, (8), 1938-1949.
8. Wesely, M. L.; Hicks, B. B., A review of the current status of knowledge on dry deposition. *Atmos. Environ.* **2000,** *34*, (12-14), 2261-2282.
9. Seinfeld, J. H.; Pandis, S. N., *Atmospheric chemistry and physics : from air pollution to climate change*. JohnWiley&Sons,Inc,Hoboken,NewJersey: Canada, 2016.
10. Guo, W. D.; Wang, X. Q.; Sun, J. N.; Ding, A. J.; Zou, J., Comparison of land-atmosphere interaction at different surface types in the mid- to lower reaches of the Yangtze River valley. *Atmospheric Chemistry and Physics* **2016,** *16*, (15), 9875-9890.
11. Brus, D.; Skrabalova, L.; Herrmann, E.; Olenius, T.; Travnickova, T.; Makkonen, U.; Merikanto, J., Temperature-Dependent Diffusion of H2SO4 in Air at Atmospherically Relevant Conditions: Laboratory Measurements Using Laminar Flow Technique. *Atmosphere* **2017,** *8*, (7), 15.
12. Wesely, M. L., Parameterization of surface resistances to gaseous dry deposition in regional-scale numerical models. *Atmos. Environ.* **1989,** *23*, (6), 1293-1304.
13. Sander, R., Compilation of Henry's law constants (version 4.0) for water as solvent. *Atmospheric Chemistry and Physics* **2015,** *15*, (8), 4399-4981.
14. Mikkonen, S.; Romakkaniemi, S.; Smith, J. N.; Korhonen, H.; Petäjä, T.; Plass-Duelmer, C.; Boy, M.; McMurry, P. H.; Lehtinen, K. E. J.; Joutsensaari, J.; Hamed, A.; Mauldin Iii, R. L.; Birmili, W.;

Spindler, G.; Arnold, F.; Kulmala, M.; Laaksonen, A., A statistical proxy for sulphuric acid concentration. *Atmospheric Chemistry and Physics* **2011,** *11*, (21), 11319-11334.
15. Lu, Y.; Yan, C.; Fu, Y.; Chen, Y.; Liu, Y.; Yang, G.; Wang, Y.; Bianchi, F.; Chu, B.; Zhou, Y.; Yin, R.; Baalbaki, R.; Garmash, O.; Deng, C.; Wang, W.; Liu, Y.; Petäjä, T.; Kerminen, V.-M.; Jiang, J.; Kulmala, M.; Wang, L., A proxy for atmospheric daytime gaseous sulfuric acid concentration in urban Beijing. *Atmospheric Chemistry and Physics* **2019,** *19*, (3), 1971-1983.
16. Holland, F.; Hofzumahaus, A.; Schafer, R.; Kraus, A.; Patz, H. W., Measurements of OH and HO2 radical concentrations and photolysis frequencies during BERLIOZ. *J. Geophys. Res.-Atmos.* **2003,** *108*, (D4), 22.
17. Holland, F.; Aschmutat, U.; Hessling, M.; Hofzumahaus, A.; Ehhalt, D. H., Highly time resolved measurements of OH during POPCORN using laser-induced fluorescence spectroscopy. *J. Atmos. Chem.* **1998,** *31*, (1-2), 205-225.
18. Lu, K. D.; Rohrer, F.; Holland, F.; Fuchs, H.; Bohn, B.; Brauers, T.; Chang, C. C.; Haseler, R.; Hu, M.; Kita, K.; Kondo, Y.; Li, X.; Lou, S. R.; Nehr, S.; Shao, M.; Zeng, L. M.; Wahner, A.; Zhang, Y. H.; Hofzumahaus, A., Observation and modelling of OH and HO2 concentrations in the Pearl River Delta 2006: a missing OH source in a VOC rich atmosphere. *Atmospheric Chemistry and Physics* **2012,** *12*, (3), 1541-1569.
19. Lu, K. D.; Hofzumahaus, A.; Holland, F.; Bohn, B.; Brauers, T.; Fuchs, H.; Hu, M.; Haseler, R.; Kita, K.; Kondo, Y.; Li, X.; Lou, S. R.; Oebel, A.; Shao, M.; Zeng, L. M.; Wahner, A.; Zhu, T.; Zhang, Y. H.; Rohrer, F., Missing OH source in a suburban environment near Beijing: observed and modelled OH and HO2 concentrations in summer 2006. *Atmospheric Chemistry and Physics* **2013,** *13*, (2), 1057-1080.
20. Tan, Z. F.; Rohrer, F.; Lu, K. D.; Ma, X. F.; Bohn, B.; Broch, S.; Dong, H. B.; Fuchs, H.; Gkatzelis, G. I.; Hofzumahaus, A.; Holland, F.; Li, X.; Liu, Y.; Liu, Y. H.; Novelli, A.; Shao, M.; Wang, H. C.; Wu, Y. S.; Zeng, L. M.; Hu, M.; Kiendler-Scharr, A.; Wahner, A.; Zhang, Y. H., Wintertime photochemistry in Beijing: observations of ROx radical concentrations in the North China Plain during the BEST-ONE campaign. *Atmospheric Chemistry and Physics* **2018,** *18*, (16), 12391-12411.
21. Tan, Z. F.; Fuchs, H.; Lu, K. D.; Hofzumahaus, A.; Bohn, B.; Broch, S.; Dong, H. B.; Gomm, S.; Haseler, R.; He, L. Y.; Holland, F.; Li, X.; Liu, Y.; Lu, S. H.; Rohrer, F.; Shao, M.; Wang, B. L.; Wang, M.; Wu, Y. S.; Zeng, L. M.; Zhang, Y. S.; Wahner, A.; Zhang, Y. H., Radical chemistry at a rural site (Wangdu) in the North China Plain: observation and model calculations of OH, HO2 and RO2 radicals. *Atmospheric Chemistry and Physics* **2017,** *17*, (1), 663-690.
22. Ma, X. F.; Tan, Z. F.; Lu, K. D.; Yang, X. P.; Liu, Y. H.; Li, S. L.; Li, X.; Chen, S. Y.; Novelli, A.; Cho, C. M.; Zeng, L. M.; Wahner, A.; Zhang, Y. H., Winter photochemistry in Beijing: Observation and model simulation of OH and HO2 radicals at an urban site. *Sci. Total Environ.* **2019,** *685*, 85-95.